



Enhanced degradation of 17 β -estradiol by AgI/N-Bi₂O₃ composite: strong synergy of adsorption–photocatalysis

Yanju Long¹ · Di Huang¹ · Lijun Luo² · Lingxin Li¹ · Lulu Wang¹ · Sifeng Zhang¹ · Fengzhi Jiang¹

Received: 29 April 2018 / Accepted: 28 July 2018 / Published online: 4 August 2018
© Springer Nature B.V. 2018

Abstract

17 β -estradiol (E2) is one of the environmental endocrine disruptors threatening human health. In this paper, AgI/N-Bi₂O₃ composites with the different mass ratio of AgI were used to remove E2 in water. The results showed that 40% AgI/N-Bi₂O₃ composite could degrade E2 by adsorption and photocatalysis synergism: 89% of E2 was adsorbed after 30 min in the dark, and E2 was completely degraded after only 10 min under visible light irradiation. Furthermore, the adsorption process of E2 can be well fitted by the pseudo-second-order kinetic model and the Langmuir model well described the E2 adsorption on the 40% AgI/N-Bi₂O₃ composite. Finally, the photocatalytic degradation dates were fitted to the pseudo-first-order kinetic model and the possible mechanism of photocatalytic degradation was proposed through the capture experiments of active species and theoretical calculations.

Keywords AgI/N-Bi₂O₃ · Adsorption–photocatalysis · 17 β -estradiol

Introduction

Environmental endocrine disrupting chemicals (EDCs) are a class of chemicals that interfere with the development of endocrine systems, normal metabolism and biological behavior [1, 2]. Many natural and synthetic chemicals are regarded as EDCs, such as bisphenol A, 17 β -estradiol (E2), and 17 α -ethynylestradiol. Among them, E2 is one of the most effective natural hormones [3]. Desbrow et al. [4] found that, when the concentration of E2 in water was greater than 0.1 ng/L, male features

Yanju Long and Di Huang have contributed equally to this work.

✉ Fengzhi Jiang
fengzhij@ynu.edu.cn

¹ School of Chemical Science and Technology, Yunnan University, Kunming 650091, China

² School of Chemistry and Biotechnology, Yunnan MinZu University, Kunming 650500, China

could be induced. So it is important for us to remove E2 in water. The removal rate of E2 by biological and physical methods is low [5, 6]. Adsorption photocatalytic synergistic degradation of pollutants is very effective [7, 8].

Semiconductor materials can be applied to many fields, including battery preparation [9], antibiotics research [10] and photocatalytic degradation [11]. Recently, bismuth-based semiconductors have attracted much interest due to their narrow band gaps and good photocatalytic activities.

Bi_2O_3 is a promising visible-light-driven photocatalyst with a narrow band gap (2.0–3.96 eV) and has different polymorphs [12, 13]. At present, the Bi_2O_3 of the alpha and beta phases are the most widely used, both of which have visible light response [14]. For example, Bi_2O_3 is used to catalyze the degradation of dyes under visible light [15, 16], and it is reported that the photocatalytic properties of Bi_2O_3 can be further enhanced by controlling the morphology [17, 18], element-doping Bi_2O_3 [19, 20] and the formation of a heterojunction composite [21, 22].

The presence of silver materials can widen the range of visible light absorption and absorption intensity, thereby improving the photocatalytic properties of materials [23–26]. In this paper, according to the characteristics of Bi_2O_3 and silver, the removal performance of N- Bi_2O_3 for E2 was improved by the formation of a heterojunction composite. Composites of AgI/N- Bi_2O_3 with the different mass ratios of AgI have been synthesized and characterized.

Experimental

Synthesis of photocatalysts

All chemicals were of analytical purity.

The N- Bi_2O_3 photocatalyst was prepared via a solvothermal–calcination method according to our previous works. In a typical synthesis, 2.42 g of $\text{Bi}(\text{NO}_3)_3 \cdot 5\text{H}_2\text{O}$ was dissolved in 20 mL of the solution containing 1.5 mL nitric acid under vigorous magnetic stirring. Then, 10 mL of ethylenediamine solution was added and the mixture solution was stirred for 30 min. Next, two drops of P123 were added and the solution was stirred for another 30 min. Then, the water bath stirring for 2 h at 80 °C to obtain a solution containing a white precipitate. The resulting solid precursor was washed with ultrapure water and absolute ethanol several times and dried at 80 °C for 12 h. Finally, the dried precursor powder was calcinated in a muffle furnace at 450 °C for 3 h to produce the N-doped Bi_2O_3 photocatalyst and was labeled as N- Bi_2O_3 .

The AgI photocatalyst was prepared via a typical procedure, when 3.0 mmol of KI was dispersed in 20 mL of deionized water and 2.7 mmol, then 15 mL of AgNO_3 solution was added dropwise, and the solution was stirred for 1 h in the dark. The resulting solid was washed with ultrapure water and absolute ethanol several times and dried at 60 °C.

The AgI/N- Bi_2O_3 photocatalysts were prepared by precipitation. An amount of 0.16 g of N- Bi_2O_3 was dispersed in 20 mL of deionized water under stirring for 30 min, and was then put into an ultrasonic bath for 20 min to make it disperse in water. Next, 3 mmol KI was added to the solution and stirred for 30 min to let the I^-

adsorb on the surface of the N-Bi₂O₃. A certain concentration of AgNO₃ solution (15 mL) was added dropwise to the above solution and stirred for 1 h in the dark. The resulting solid precursor was washed with ultrapure water and absolute ethanol several times and dried at 60 °C for 8 h to achieve the AgI/N-Bi₂O₃ photocatalyst. The AgI/N-Bi₂O₃ photocatalyst with the AgI mass ratio in total masses of 20, 40, 60 and 80% were obtained by controlling the amount of AgNO₃, and were labeled as 20% AgI/N-Bi₂O₃, 40% AgI/N-Bi₂O₃, 60% AgI/N-Bi₂O₃ and 80% AgI/N-Bi₂O₃, respectively.

Characterization

The crystal structures of the sample powders were characterized by TTRIII X-ray diffractometer (XRD; Rigaku, Japan) with Cu K α radiation and an applied current of 40 kV and 200 mA. The morphologies were observed on a FEI QUANTA200 scanning electron microscope (SEM; FEI, USA) and a Tecnai G² TF30 S-Twin field-emission transmission electron microscope (FE-TEM; FEI, Holland). The elemental composition was analyzed using a PHI5000 Versaprobe scanning XPS microprobe (XPS; ULVAC-PHI, Japan). Nitrogen adsorption–desorption measurement at 77 K was conducted using a TriStar II 3020 (BET; Micromeritics, USA). The surface area of the samples was obtained using the Brunauer–Emmett–Teller plot of the N₂ adsorption isotherm. The ultraviolet–visible diffuse reflectance spectra were recorded at room temperature on a UV-240IPC spectrophotometer (UV–Vis DRS; JEOL, Japan) by using BaSO₄ as a reference. The photoluminescence emission spectra were collected on a F-70000 fluorescence spectrophotometer (PL; Hitachi, Japan) with the exciting light of a wavelength of 350 nm.

Adsorption degradation measurements

An adsorption kinetic study was carried out by mixing 5 mg of the 40% AgI/N-Bi₂O₃ composites and 10 mL 3 mg/L E2 solution at 298 K in an XPA-7 photochemical reactor (Xujiang Electromechanical Plant, Nanjing, China) in the dark. The suspension solution was taken at pre-determined time intervals (2, 4, 8, 12, 21 and 30 min), filtered through a 0.45- μ m filter to remove the photocatalyst particles and subjected to subsequent HPLC (Waters, USA) analysis. The mobile-phase composition was acetonitrile/water (55/45, v/v) at a flow rate of 0.4 mL/min. The column temperature was 45 °C and the injection volume was 7 μ L. The following equations were used to model the adsorption kinetics of the E2:

The amount of E2 adsorbed onto photocatalysts:

$$q_e(\text{mg/g}) = (C_0 - C_q) V/m \quad (1)$$

$$q_t(\text{mg/g}) = (C_0 - C_t) V/m \quad (2)$$

The pseudo-first-order equation:

$$\ln(q_e - q_t) = \ln q_e - k_1 t \quad (3)$$

The pseudo-second-order equation:

$$t/q_t = 1/k_2q_e^2 + t/q_e \quad (4)$$

q_e (mg/L), q_t (mg/L), C_0 (mg/L), C_q (mg/L), C_t (mg/L) and m (g) represent the amounts of E2 adsorbed at the equilibrium, the amounts of E2 adsorbed at time t (min), the initial concentration of E2, the concentration of E2 when the adsorption equilibrium was established, the concentration of E2 in solution at adsorption time t (min) and the weight of the photocatalyst used, respectively. k_1 and k_2 are kinetics constants.

Adsorption isotherm study also was carried out by mixing 5 mg of the 40% AgI/N-Bi₂O₃ composites and E2 solution with initial concentrations of 1, 3, 5, 7 and 9 mg/L at 298 K. The concentrations of the E2 were analyzed after the adsorption was run for 30 min. The following equations were used to model the adsorption isotherm of E2:

$$\text{The Langmuir model: } 1/q_e = 1/q_m k_L C_q + 1/q_m \quad (5)$$

$$\text{The Freundlich model: } \ln q_e = \ln k_F + \ln C_q/n \quad (6)$$

k_L , k_F , n and q_m (mg/L) are the Langmuir constant, the Freundlich constant, the Freundlich exponent and the maximum adsorption quantity of E2, respectively.

Photocatalytic activity measurements

In order to clarify the adsorption removal rate and the photodegradation removal rate, we have taken 30 min as the dark adsorption time before the photocatalytic reaction. The photocatalytic degradation experiments were conducted in an XPA-7 photochemical reactor with the quartz tubes around the lamp. The exciting light was generated by a 500-W Xe lamp and a 420-nm cutoff filter (cutting off the UV light) to obtain visible light. In each test, 5.0 mg photocatalyst was added to a quartz tube with 10.0 mL of E2 solution (3 mg/L). Prior to the irradiation, the solution was stirred in the dark for 30 min to establish the adsorption equilibrium. Then, under the visible light irradiation, the quartz tube was taken out at given time intervals and the residual concentration of E2 was determined. The degradation efficiency of E2 was as follows:

$$\text{Removal rate of E2 (\%)} = (C_0 - C)/C_0 \times 100\% \quad (7)$$

$$\text{Adsorption removal rate (\%)} = (C_0 - C_q)/C_0 \times 100\% \quad (8)$$

$$\text{Photocatalysis removal rate (\%)} = (C_q - C)/C_0 \times 100\%, \quad (9)$$

where C (mg/L) is the concentration of E2 in solution at irradiation time t (min).

A pseudo-first-order kinetic model was used to evaluate the photodegradation efficiency, and the degradation kinetics constant, k , was obtained, as in Eq. (10):

$$\ln(C/C_q) = -kt \quad (10)$$

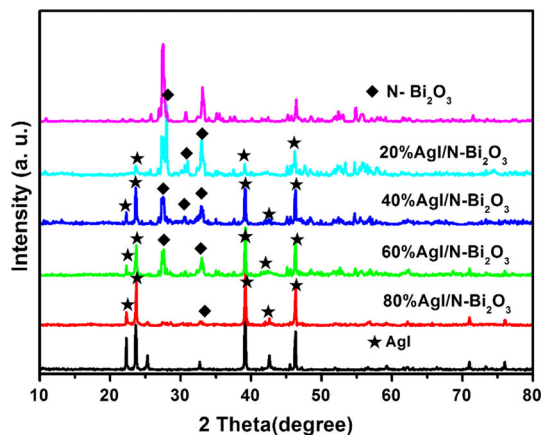
Results and discussion

Characterization

In order to investigate the chemical composition and phase structure of the photocatalysts, they were characterized by XRD. As shown in Fig. 1, the diffraction peaks of pure N-Bi₂O₃ at the 2 θ values of 26.9°, 27.3°, 45.1°, 46.3°, 52.4°, 57.8°, 57.9° and 59.0° were observed, and matched well with the (111), (120), (023), (041), (-321), (024), (051) and (150) crystal planes of α -Bi₂O₃, respectively (JCPDS No. 41-1449), and at 2 θ values of 30.7° matched well with the (008) crystal plane of Bi₅O₇NO₃ (JCPDS No. 51-0525). This indicated that pure N-Bi₂O₃ was a mixed-crystal consisting with the two α -Bi₂O₃ and Bi₅O₇NO₃ phases. In other words, N replaces some of the O atoms in the Bi₂O₃ lattice, entering the crystal phase [27]. Meanwhile, the diffraction peaks of pure AgI at the 2 θ values of 22.3°, 23.7°, 25.3°, 32.7°, 39.2°, 42.6°, 45.6°, 46.3°, 71.0° and 76.1° were observed, which matched well with the (100), (002), (101), (102), (110), (103), (200), (112), (300) and (302) crystal planes, respectively, of the AgI standard card (JCPDS 09-0374). Furthermore, no other diffraction peaks were observed, indicating the high purity of the samples. For the AgI/N-Bi₂O₃ composites, the diffraction peaks of AgI become stronger with increasing the mass ratio of AgI from 20 to 80%, while the characteristic peaks of N-Bi₂O₃ were decreased in intensity. That is, the AgI was successfully loaded onto the N-Bi₂O₃ surface to form the AgI/N-Bi₂O₃ photocatalysts.

XPS measurement was carried out to examine the surface chemical states and compositions of the elements in the 40% AgI/N-Bi₂O₃ photocatalyst. Figure 2a shows a typical XPS survey spectrum of the 40% AgI/N-Bi₂O₃ photocatalyst, in which all the peaks can be assigned to the Bi, O, N, Ag, I and C elements, and C was the external carbon introduced by the instrument calibration. Figure 2b shows high-resolution XPS spectra of Bi 4f. The Bi 4f_{7/2} peak at 158.8 eV and Bi 4f_{5/2} at 164.2 eV can be observed with a separation of 5.4 eV, which was a characteristic of

Fig. 1 XRD patterns of the photocatalysts with different mass ratios of AgI



Bi^{3+} according to the previous report [25, 28]. Figure 2c presents the high-resolution O 1s spectrum, which can be deconvoluted into three peaks, namely oxygen in the lattice (Bi–O–Bi) at 528.6 eV, oxygen in the lattice (Bi–O) at 531.0 eV and oxygen in the lattice (N–O) at 530.1 eV [29]. Figure 2d shows high-resolution XPS spectra of I 3d, in which the I 3d_{5/2} peak at 619.2 eV and the I 3d_{3/2} peak at 630.8 eV can be observed, a characteristic of I⁻ according to the previous reports [30]. Figure 2e shows high-resolution XPS spectra of Ag 3d, in which the Ag 3d_{5/2} peak at 368.2 eV and the Ag 3d_{3/2} peak at 374.0 eV can be observed, a characteristic of Ag⁺ according to the previous reports [30]. Figure 2f shows a weak

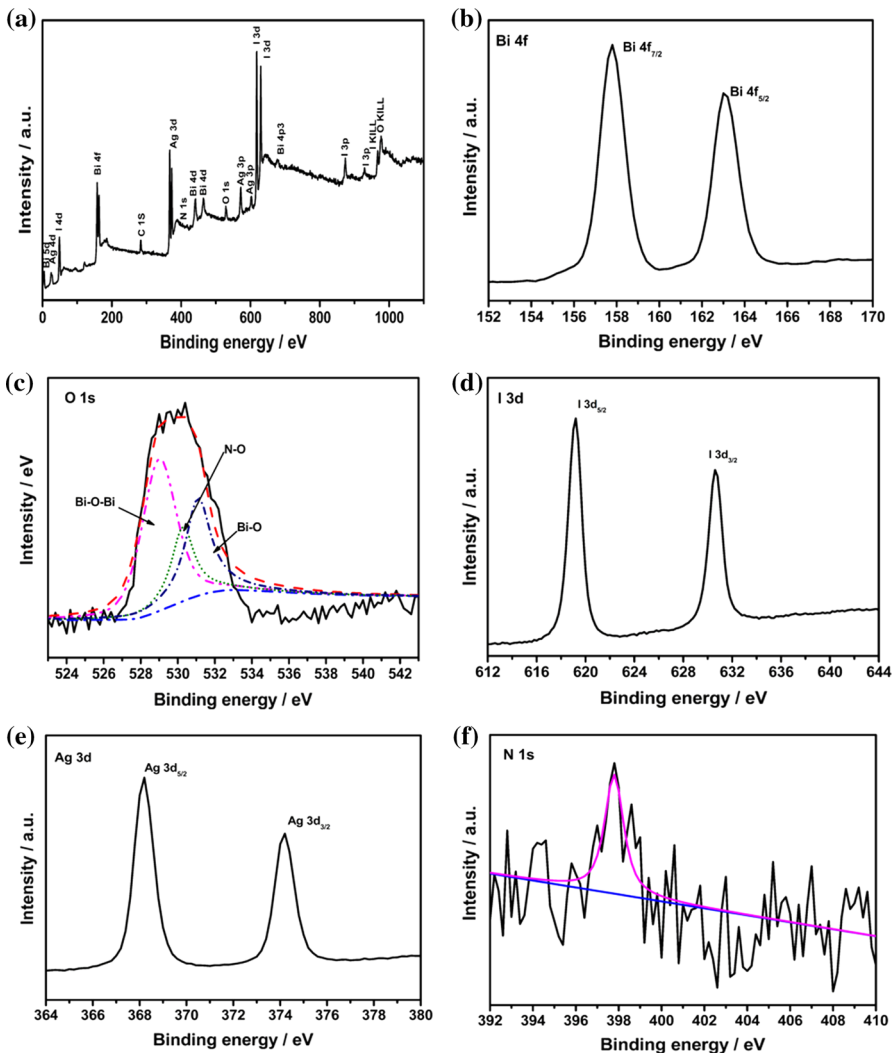


Fig. 2 XPS survey spectra of 40% AgI/N-Bi₂O₃ (a), Bi 4f spectra (b), O 1s spectra (c), I 3d spectra (d), Ag 3d spectra (e), and N 1s spectra (f)

peak of N 1s in the binding energy of 397.4 eV caused by the N atom in NO³⁻. Therefore, the XPS results further confirms the coexistence of N-Bi₂O₃ and AgI in the AgI/N-Bi₂O₃ heterostructure.

The morphology and surface structure of N-Bi₂O₃, AgI and the AgI/N-Bi₂O₃ photocatalysts with the different mass ratios of AgI were studied by SEM. It can be seen in Fig. 3a that the morphology of N-Bi₂O₃ was an irregular sheet structure. Figure 3f shows the morphology of AgI, and it can be seen that AgI was tanhe irregular cluster, composed of small particles. Figure 3b–d shows the morphology of 20% AgI/N-Bi₂O₃, 40% AgI/N-Bi₂O₃ and 60% AgI/N-Bi₂O₃, and it can be seen that the N-Bi₂O₃ surface of nanosheets become rougher when covered by the continuously growing AgI particles. Figure 3e shows the morphology of 80% AgI/N-Bi₂O₃, and it can be seen that the nanosheet structure disappears completely, because the AgI content was very high and the sheet structure was completely wrapped by AgI to form the larger particles, further indicating that the photocatalyst was AgI/N-Bi₂O₃.

From the TEM images in Fig. 4a, b, we can see that the AgI was composed of small particles and the N-Bi₂O₃ was in sheets. The TEM of the 40% AgI/N-Bi₂O₃ photocatalyst are shown in Fig. 4c, from which it can be seen that the AgI particles were deposited on the surface of the N-Bi₂O₃ sheets. This proves that the composite of the AgI/N-Bi₂O₃ was successfully prepared.

N₂ adsorption–desorption isotherms were calculated to investigate the surface area and pore structures of the obtained 40% AgI/N-Bi₂O₃. As shown in Fig. 4d, the isotherms belong to type IV with an H3 hysteresis loop, a characteristic of

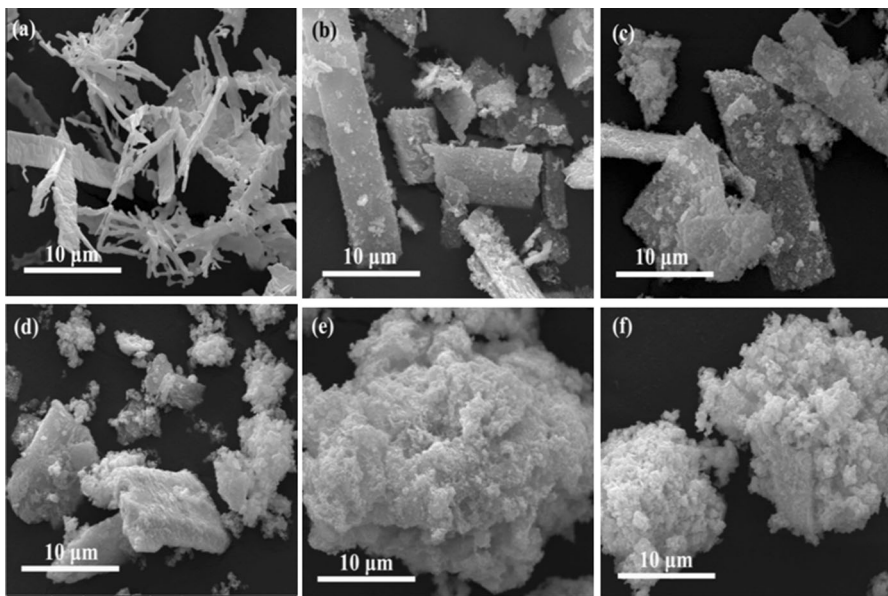


Fig. 3 SEM images of photocatalysts: N-Bi₂O₃ (a), 20% AgI/N-Bi₂O₃ (b), 40% AgI/N-Bi₂O₃ (c), 60% AgI/N-Bi₂O₃ (d), 80% AgI/N-Bi₂O₃ (e), and AgI (f)

mesoporous materials. The BET surface areas of 40% AgI/N-Bi₂O₃ were estimated using N₂ isotherms to be 6.63 m²/g, and the average pore size was calculated to be 10.75 nm.

The UV–Vis DRS of the samples were investigated to probe their optical properties. As shown in Fig. 5a, N-Bi₂O₃ shows absorption edges at about 440 nm, and the AgI/N-Bi₂O₃ photocatalysts with the different mass ratio of AgI show absorption edges greater than 440 nm, while the intensity of the absorption peak also increased with the increase of the AgI mass ratio. The results shows that AgI can improve the visible light utilization of the materials and improve their photocatalytic activity.

The optical absorption performance of a semiconductor is evaluated based on band gap energy (E_g), which was evaluated using Eq. (11):

$$\alpha h\nu = k(h\nu - E_g)^{n/2}, \quad (11)$$

where α , h , ν , k and E_g represent the absorption coefficient, Planck constant, light frequency, a constant and band gap energy, respectively. The absorbance (A) of the photocatalyst is proportional to its absorption coefficient (α), and the value of n

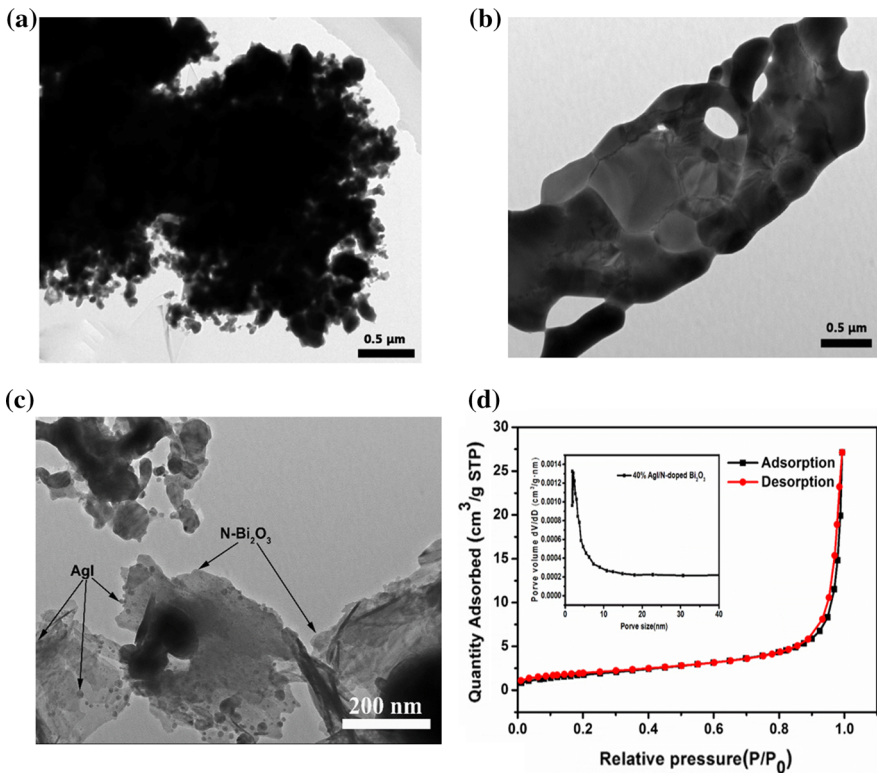


Fig. 4 TEM images of AgI (a), N-Bi₂O₃ (b), 40% AgI/N-Bi₂O₃ (c) and N₂ adsorption–desorption isotherm curves of 40% AgI/N-Bi₂O₃ (d)

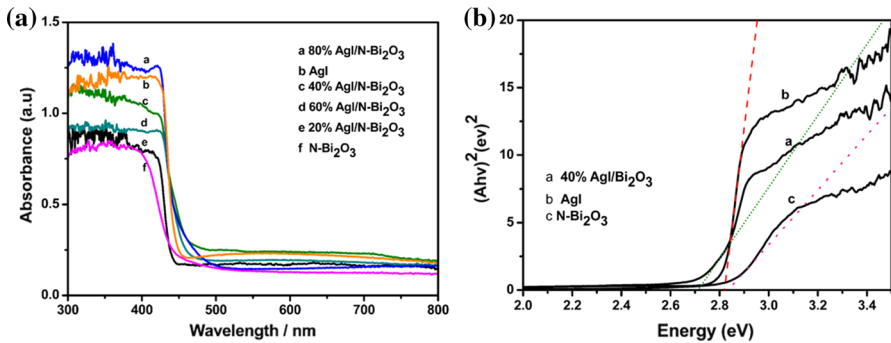


Fig. 5 Uv-vis adsorption spectra of photocatalysts with different mass ratios of AgI (a) and the plots of $(Ah\nu)^2$ versus energy $(h\nu)$ for the band gap energy of the photocatalysts (b)

depends on the characteristic of the transition in a semiconductor, being 1 for Bi₂O₃ [31] and 1 for AgI [32].

The band gap energies of N-Bi₂O₃, AgI and 40% AgI/N-Bi₂O₃ were estimated to be about 2.83, 2.79 and 2.71 eV from the plot of $(Ah\nu)^2$ versus energy $(h\nu)$ in Fig. 5b, respectively. The results show that the band gap of the composited AgI/N-Bi₂O₃ decreased compared to the two pure photocatalysts.

The relative band positions of N-Bi₂O₃ and AgI were investigated by the following empirical formulae:

$$E_{VB} = \chi - E^c + 0.5E_g \quad (12)$$

$$E_{CB} = E_{VB} - E_g \quad (13)$$

In these equations, χ is the absolute electronegativity of the semiconductor, and the values of Bi₂O₃ and AgI are 6.23 [32] and 5.48 eV [25], respectively. E^c is the energy of free electrons on the hydrogen scale (about 4.5 eV) and E_g is the band gap energy of the semiconductor. E_{VB} and E_{CB} stand for the valence band (VB) and conduction band (CB) edge potential, respectively. Consequently, the E_{CB} of N-Bi₂O₃ and AgI were calculated to 0.31 and -0.41 eV, respectively, and the E_{VB} of N-Bi₂O₃ and AgI were 3.14 and 2.38 eV, respectively.

In order to study the recombination ability of the photogenerated electrons and holes, the solid fluorescence spectrum was used to characterize the material [22], and the results are shown in Fig. 6. With the increased content of AgI, the absorption peak decreased gradually, suggesting that the addition of AgI can inhibit the photogenerated electron-hole recombination, and improve the photocatalytic performance of the materials.

Adsorption degradation experiments

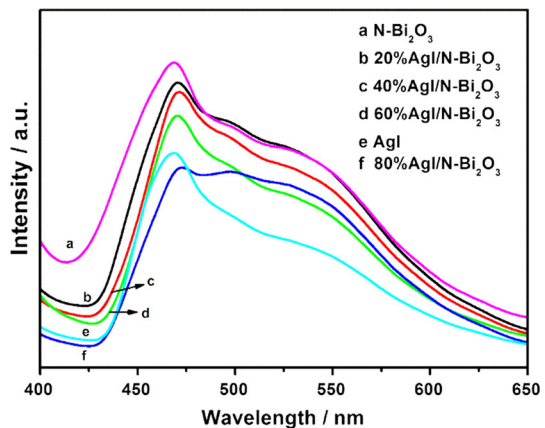
Adsorption kinetics study

The results of the study of the adsorption kinetics of E2 are illustrated in Fig. 7. The adsorption amount of E2 is shown in Fig. 7a and it can be seen that the adsorption balance can be established in about 30 min for the removal of E2 over the 40% AgI/N-Bi₂O₃ and the amounts of E2 adsorbed at the equilibrium q_e is 5.23 mg/g. The pseudo-first- and pseudo-second-order kinetic models were used to analyze the adsorption data based on Eqs. (3) and (4). The constant k_1 of the pseudo-first-order was 0.211 based on the intercepts of the plots of $\ln(q_e - q_t)$ versus t (Fig. 7b) and the constant k_2 of the pseudo-second-order was 0.076 based on the intercept of plots of $1/q_t$ versus t (Fig. 7c). At the same time, the correlation coefficients for the pseudo-first- and pseudo-second-order kinetic models were 0.988 and 0.996. These results demonstrate that the adsorption process of E2 on the 40%AgI/N-Bi₂O₃ photocatalyst can be well fitted by the pseudo-second-order kinetic model.

Adsorption isotherm study

The influence of the initial concentration of E2 solution on the adsorbing capacity is shown in Fig. 8a. The adsorbing capacity of the 40% AgI/N-Bi₂O₃ photocatalyst increased with the increased initial concentration of E2 solution. The Langmuir and Freundlich equations are commonly used to study adsorption isotherms. According to Eqs. (5) and (6), the modeled results are shown in Fig. 8b, c. The Langmuir constant rate k_L was 7.69 based on the slope of the plots of $1/q_e$ versus $1/C_q$ (Fig. 8b), and the Freundlich constant k_F was 6.46 based on the intercept of the plots of $\ln q_e$ versus $\ln C_q$ (Fig. 8c). In addition, the correlation coefficients for the Langmuir and the Freundlich equations were 0.989 and 0.982. The result was that the Langmuir equation can be used to describe the adsorption process of E2 on the 40% AgI/N-Bi₂O₃ photocatalyst. However, the Freundlich model was not suitable for the E2 adsorption on the 40% AgI/N-Bi₂O₃ photocatalyst.

Fig. 6 PL spectra of photocatalysts with the different mass ratios of AgI



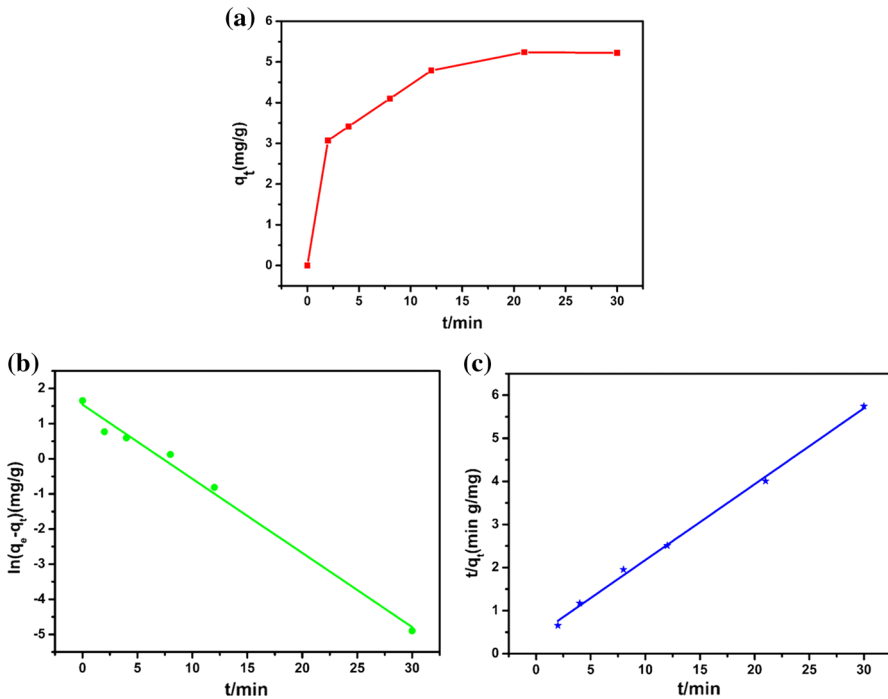


Fig. 7 Experimental data of the adsorbed amounts of E2 on the 40% AgI/N-Bi₂O₃ photocatalyst versus time (a), the linear fit pseudo-first-order kinetic model (b) and the pseudo-second-order kinetic model (c)

Photocatalytic degradation experiments

The adsorption capacity and catalytic performance of N-Bi₂O₃, AgI and AgI/N-Bi₂O₃ composite photocatalysts for E2 were studied. Firstly, as Fig. 9a shows, the E2 was only slightly degraded without photocatalysts, indicating that the photolysis of E2 could be ignored. It can also be clearly observed that the removal ratio of E2 was significantly increased using 40% AgI/N-Bi₂O₃ as the photocatalyst compared to pure AgI and pure N-Bi₂O₃. To further study the photocatalytic activity of the photocatalyst, the photocatalytic degradation data were fitted to a pseudo-first-order kinetics model and the k values calculated based on Eq. (10). The results shown in Fig. 9b illustrate that the reaction kinetics of the photocatalysts could be well fitted by the pseudo-first-order rate model. The calculated k values of AgI, N-Bi₂O₃ and 40% AgI/N-Bi₂O₃ were 0.0638, 0.0293, 0.2014 min⁻¹, respectively. The rate constants of 40% AgI/N-Bi₂O₃ were 3.16 and 6.87 times of AgI and N-Bi₂O₃, respectively.

Secondly, the photocatalytic properties of AgI/N-Bi₂O₃ composites with different mass ratios of AgI were compared. As Fig. 9c shows, the E2 reached the adsorption equilibrium in the dark for 30 min, and the adsorption removal rates of 20% AgI/N-Bi₂O₃, 40% AgI/N-Bi₂O₃, 60% AgI/N-Bi₂O₃, 80% AgI/N-Bi₂O₃ and AgI were 9, 89, 25, 51 and 10%, respectively. Also, under visible light irradiation

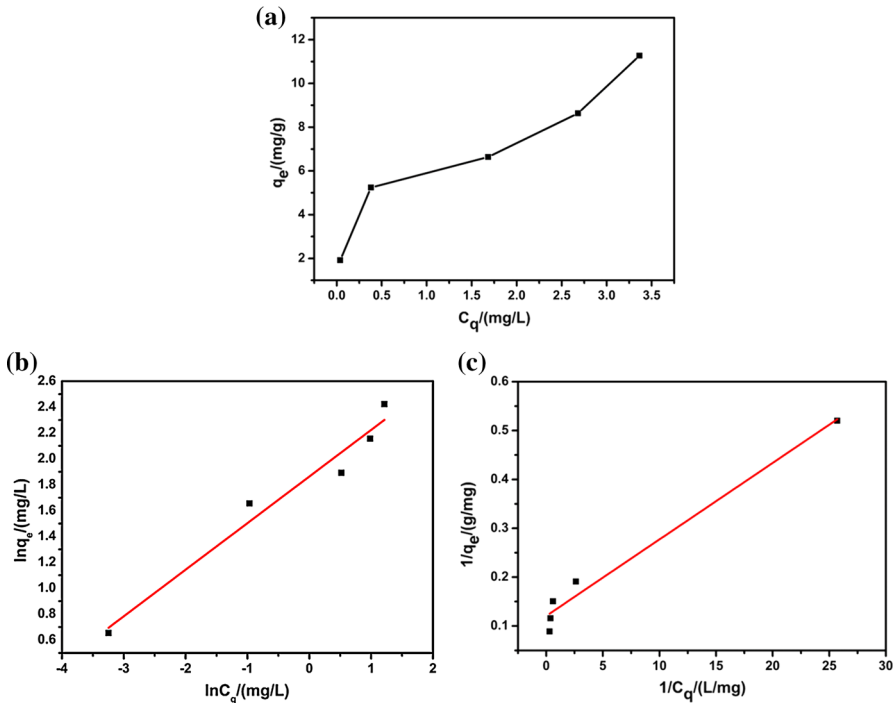


Fig. 8 The result of the initial concentration on adsorbed E2 (a), linear fitting of experimental data using the Freundlich (b) and Langmuir (c) sorption isotherms

for 10 min, the removal rates of E2 were 57, 100, 90, 97 and 48%, respectively. E2 was rapidly degraded by visible light irradiation after adsorption on the catalyst. It can be seen that 40% AgI/N-Bi₂O₃ had a strong adsorption capacity for E2. As Table 1 shows, the specific surface area of 40% AgI/N-Bi₂O₃ was the largest in all the materials, which would help to provide more active sites. The chemical force between Ag⁺ of AgI/N-Bi₂O₃ and phenolic hydroxyl of E2 may enhance the adsorption of E2 compared with N-Bi₂O₃ [33]. Therefore, the chemical force and specific surface area may be the factors affecting adsorption performance. Furthermore, broadening the range of visible light absorption was also the reason for the improvement of the photocatalytic performance. Thus, the 40% AgI/N-Bi₂O₃ composite was selected as the optimized material.

In order to investigate the photochemical stability of the 40% AgI/N-Bi₂O₃, the recycling experiments were carried out for the photodegradation of E2, and the results are shown in Fig. 10a. In addition, the photocatalysts after the photocatalytic reaction of four cycles was examined by XRD and XPS, as shown in Figs. 8b and 10c. From Fig. 10a, we can see that the removal rate of E2 over the 40% AgI/N-Bi₂O₃ photocatalyst decreased from 100 to 95.8% after four cycles. As shown in Fig. 10b, the diffraction peaks at 2θ values of 38.1°, 64.5° and 77.5° were observed in the 40% AgI/N-Bi₂O₃ photocatalyst after four cycles, which belong to the characteristic peaks of Ag (JCPDS 04-0783). The results show that part of the AgI

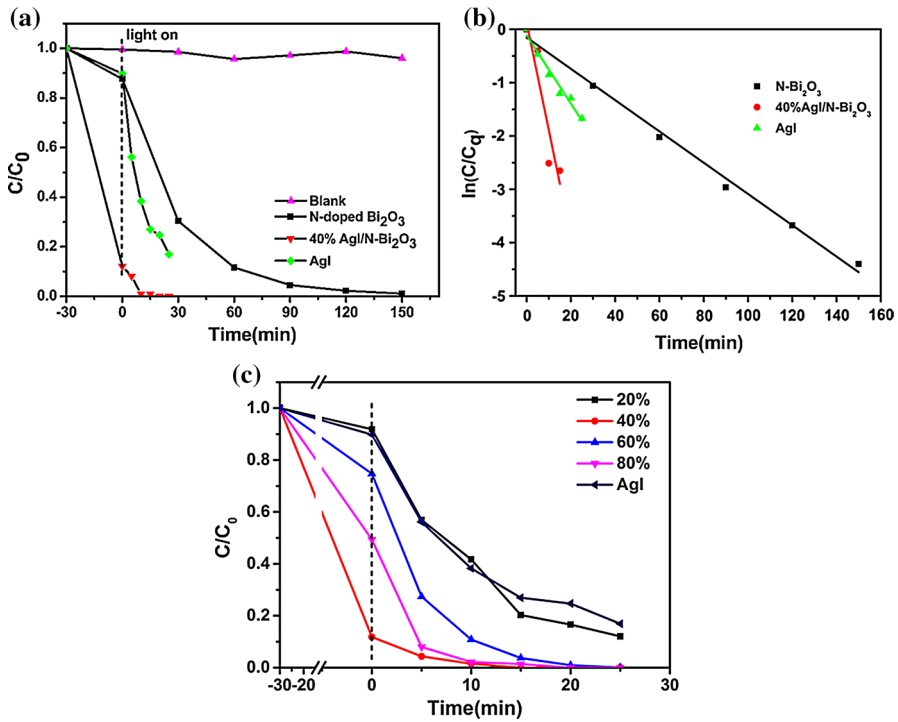


Fig. 9 Photocatalytic degradation of E2 with different photocatalysts (a), the corresponding fitted plots of pseudo-first-order kinetics (b) and photocatalytic degradation of E2 with different mass ratios of AgI (c)

Table 1 Specific surface area of photocatalysts

Semiconductor	Specific surface area (m ² /g)
N-Bi ₂ O ₃	2.84
20% AgI/N-Bi ₂ O ₃	3.69
40% AgI/N-Bi ₂ O ₃	6.63
60% AgI/N-Bi ₂ O ₃	4.50
80% AgI/N-Bi ₂ O ₃	3.78
AgI	1.80

in the 40% AgI/N-Bi₂O₃ photocatalyst were reduced to Ag after four cycles. Figure 10c, d shows that the Ag 3d_{5/2} was shifted to the higher binding energy region by 0.2 eV, and the Ag 3d_{3/2} was shifted to the lower by 0.4 eV after four cycles, and peaks at 368.6 and 374.6 eV were observed, which belong to the Ag. This proved again that part of the AgI were reduced to Ag in the 40% AgI/N-Bi₂O₃ photocatalyst after four cycles.

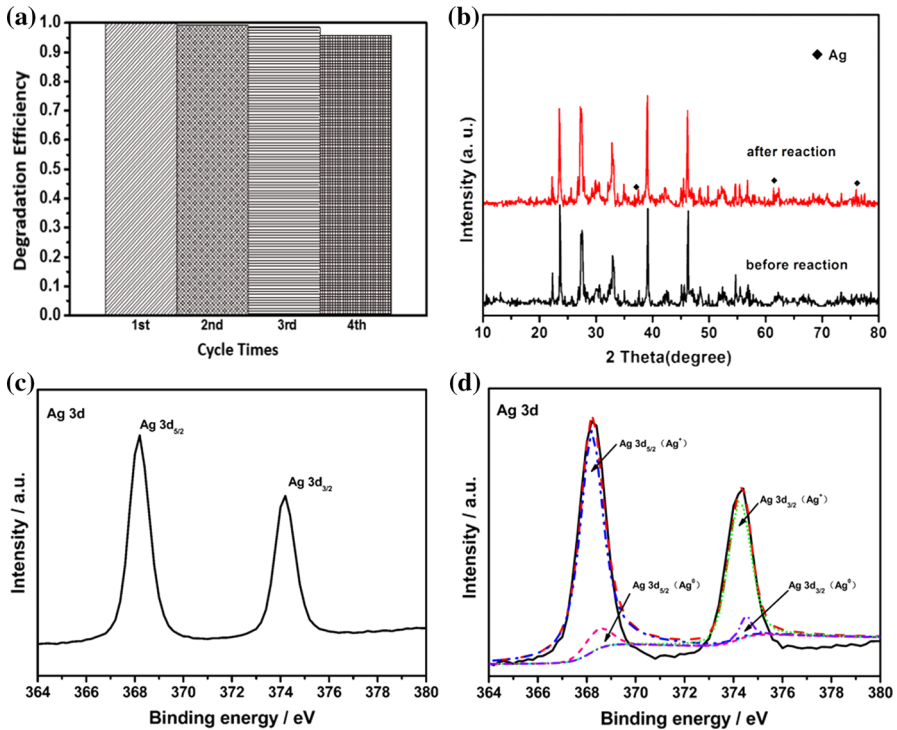


Fig. 10 Recycling photodegradation of E2 over 40% AgI/N-Bi₂O₃ (a), XRD patterns of 40% AgI/N-Bi₂O₃ before and after recycling photocatalytic reaction (b), and XPS Ag 3d spectra of 40% AgI/N-Bi₂O₃, before (c) and after (d) recycling photocatalytic reactions

Photocatalytic mechanism

Usually, the active species including superoxide radical ($\cdot\text{O}_2^-$), holes (h^+), and hydroxyl radical ($\cdot\text{OH}$) has strong oxidation ability in the photocatalytic degradation process. In order to investigate the active species generated over 40% AgI/N-Bi₂O₃, trapping experiments were performed. 4-benzoquinone (BQ), ammonium oxalate (AO) and isopropyl alcohol (IPA) were applied as h^+ scavengers, $\cdot\text{O}_2^-$ scavenger and $\cdot\text{OH}$ scavenger, respectively [34]. As seen in Fig. 11, the addition of all the scavengers made the degradation efficiency of E2 decrease. Especially, the presence of BQ made the removal rate of E2 significantly decrease, which indicated that $\cdot\text{O}_2^-$ was the main active species, while h^+ and $\cdot\text{OH}$ also played important roles in the photocatalytic reaction.

Based on the above experimental results, a possible photocatalytic mechanism is as illustrated in Fig. 12. When the 40% AgI/N-Bi₂O₃ photocatalyst was irradiated by visible light, both AgI and N-Bi₂O₃ could be excited, and electrons and holes located at CB and VB of AgI and N-Bi₂O₃, respectively. The CB position of AgI (-0.41 eV) was more negative than the standard redox potentials of $\text{O}_2/\cdot\text{O}_2^-$ (0.13 eV) [35], indicating that electrons on the CB of AgI could be captured by the

Fig. 11 Effect of different reactive species scavengers on the photodegradation of E2 over 40% AgI/N-Bi₂O₃

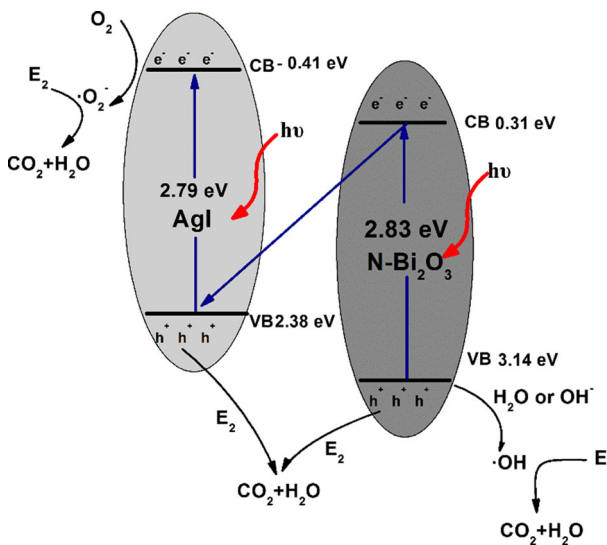
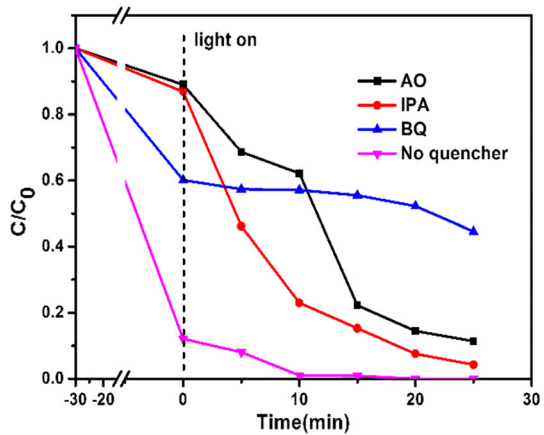
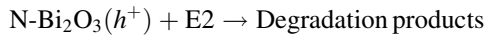
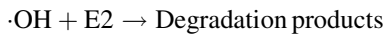
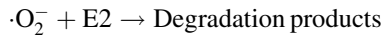
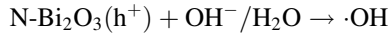
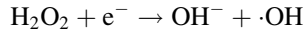
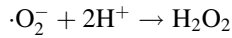
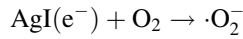
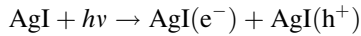
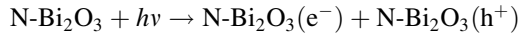


Fig. 12 The possible photocatalytic mechanism of the 40% AgI/N-Bi₂O₃ photocatalyst

absorbed O₂ to generate reactive ·O₂⁻. However, the E_{CB} of N-Bi₂O₃ (0.31 eV) was higher than E(O₂/·O₂⁻) and the ·O₂⁻ could not be produced on the CB of N-Bi₂O₃. The E_{CB} of N-Bi₂O₃ (0.31 eV) was higher than E_{CB} of AgI (-0.41 eV), so the electrons on the CB of N-Bi₂O₃ would transfer to the VB of AgI, and recombine with the holes on the VB of AgI. Ag⁺ combined with the electrons on the CB of N-Bi₂O₃ and was reduced to Ag. These led to the electrons on the CB of AgI and the holes on the VB of N-Bi₂O₃ becoming well separated. The VB of N-Bi₂O₃ (3.14 eV) was higher than E(·OH/OH⁻ = 2.68 eV) [35], so the photo-generated holes on the VB of N-Bi₂O₃ could oxidize OH⁻ to yield ·OH. Finally, ·OH, ·O₂⁻ and h⁺ could degrade pollutants altogether. The possible reactions in the photodegradation process of E2 were as follows:



Conclusion

In this work, AgI/N-Bi₂O₃ composites with different mass ratios of AgI were successfully prepared by a precipitation method. The crystal phase, surface chemical states and compositions, morphology and optical properties of AgI/N-Bi₂O₃ were investigated in detail. The results showed that the composite of AgI and N-Bi₂O₃ would enhance the visible light utilization, increase the specific surface area and reduce the combination of electron–hole pairs, and these would enhance the activity of the AgI/N-Bi₂O₃ composite. The 40% AgI/N-Bi₂O₃ composite could degrade E2 by the adsorption and photocatalysis synergism: 89% of E2 was adsorbed after 30 min in the dark, and E2 was completely degraded after only 10 min under visible light irradiation. Part of the AgI was reduced to Ag in the 40% AgI/N-Bi₂O₃ photocatalyst after four cycles of photodegradation. The possible photocatalytic mechanism has also been discussed according to the band gap energy, conduction band position, valence band position and active species. It was proved that 40% Ag/N-Bi₂O₃ was an effective photocatalyst for the degradation of E2.

Acknowledgement This work was supported by National Natural Science Foundation of China (Nos. 21763032, 21261026 and 21767030) and Major Project of Kunming Science and Technology Bureau (No. 2017-1-S-12305).

References

1. C.G. Daughton, T.A. Ternes, *Environ. Health Perspect.* **107**, 907 (1999)
2. M.L. Janex-Habibi, A. Huyard, M. Esperanza, A. Bruchet, *Water Res.* **43**, 1565 (2009)
3. R.R. Chowdhury, P.A. Charpentier, M.B. Ray, *J. Photochem. Photobiol. A* **219**, 67 (2011)
4. C. Desbrow, E.J. Routledge, G.C. Brighty, *Environ. Sci. Technol.* **32**, 1549 (1998)
5. Y. Yoon, P. Westerhoff, J. Yoon, S.A. Snyder, *J. Environ. Eng.* **130**, 1460 (2004)
6. P. Blaquez, B. Guieysse, *J. Hazard. Mater.* **150**, 459 (2008)
7. X. Zheng, S. Xu, Y. Wang, X. Sun, Y. Gao, B. Gao, *J. Colloid Interface Sci.* **527**, 202 (2018)
8. L. Qi, K. Dong, T. Zeng, J. Liu, J. Fan, X. Hu, W. Jia, E. Liu, *Catal. Today* **314**, 42 (2018)
9. H. Liu, H. Guo, B. Liu, M. Liang, Z. Lv, K.R. Adair, X. Sun, *Adv. Funct. Mater.* **28**, 1707480 (2018)
10. L. Hu, J. Wan, G. Zeng, A. Chen, G. Chen, Z. Huang, K. He, M. Cheng, C. Zhou, W. Xiong, C. Lai, P. Xu, *Environ. Sci. Nano* **4**, 2018 (2017)
11. C. Zhou, C. Lai, D. Huang, G. Zeng, C. Zhang, M. Cheng, L. Hu, J. Wan, W. Xiong, M. Wen, X. Wen, L. Qin, *Appl. Catal. B* **220**, 202 (2018)
12. J. Sun, X. Li, Q. Zhao, M.O. Tadé, S. Liu, *Appl. Catal. B* **219**, 259 (2017)
13. Y. Wang, Y. Wen, H. Ding, Y. Shan, *J. Mater. Sci.* **45**, 1385 (2009)
14. J. Eberl, H. Kisch, *Photochem. Photobiol. Sci.* **7**, 1400 (2008)
15. S. Iyyapushpam, S.T. Nishanthi, D. Pathinettam Padiyan, *J. Alloys Compd.* **563**, 104 (2013)
16. Y. Yan, Z. Zhou, Y. Cheng, L. Qiu, C. Gao, J. Zhou, *J. Alloys Compd.* **605**, 102 (2014)
17. M. Vila, C. Díaz-Guerra, J. Piqueras, *J. Alloys Compd.* **548**, 188 (2013)
18. C. Wu, L. Shen, Q. Huang, Y.-C. Zhang, *Mater. Lett.* **65**, 1134 (2011)
19. X. Zhong, Z. Dai, F. Qin, *R. Soc. Chem.* **5**, 69312 (2015)
20. W. Xiaohong, Q. Wei, L. Li, G. Yun, X. Zhaoyang, *Catal. Commun.* **10**, 600 (2009)
21. F. Qin, G. Li, R. Wang, J. Wu, H. Sun, R. Chen, *Chemistry* **18**, 16491 (2012)
22. W. Gou, P. Wu, D. Jiang, X. Ma, *J. Alloys Compd.* **646**, 437 (2015)
23. B. Song, Q. Tang, Q. Li, W. Wu, H. Zhang, J. Cao, M. Ma, *Mater. Lett.* **209**, 622 (2017)
24. J. Liang, F. Liu, J. Deng, M. Li, M. Tong, *Water Res.* **123**, 632 (2017)
25. Z. Xiang, Y. Wang, P. Ju, Y. Long, D. Zhang, *J. Alloys Compd.* **721**, 622 (2017)
26. C. Zhou, C. Lai, P. Xu, G. Zeng, D. Huang, C. Zhang, M. Cheng, L. Hu, J. Wan, Y. Liu, W. Xiong, Y. Deng, M. Wen, *ACS Sustain. Chem. Eng.* **6**, 4174 (2018)
27. Y.Y.-C. LU Yuan-Gang, YE Zhi-Xiang, LIU Sheng-Yu, *Journal of Inorganic Materials* **27** (2012)
28. Z. Bian, J. Zhu, S. Wang, Y. Cao, X. Qian, H. Li, *J. Phys. Chem. C* **112**, 6259 (2008)
29. S. Gong, Q. Han, X. Wang, J. Zhu, *CrystEngComm* **17**, 9185 (2015)
30. Y. Liang, H. Wang, L. Liu, P. Wu, W. Cui, J.G. McEvoy, Z. Zhang, *J. Mater. Sci.* **50**, 6935 (2015)
31. X. Xiao, R. Hu, C. Liu, C. Xing, C. Qian, X. Zuo, J. Nan, L. Wang, *Appl. Catal. B* **140**, 433 (2013)
32. Q. Yang, J. Huang, J. Zhong, J. Chen, J. Li, S. Sun, *Curr. Appl. Phys.* **17**, 1202 (2017)
33. X. Ji, G. Kan, X. Jiang, B. Sun, M. Zhu, Y. Sun, *J. Colloid Interface Sci.* **523**, 98 (2018)
34. C. Zhou, C. Lai, P. Xu, G. Zeng, D. Huang, Z. Li, C. Zhang, M. Cheng, L. Hu, J. Wan, F. Chen, W. Xiong, R. Deng, *ACS Sustain. Chem. Eng.* **6**, 6941 (2018)
35. Y. Chen, G. Tian, Y. Shi, Y. Xiao, H. Fu, *Appl. Catal. B* **164**, 40 (2015)